Nanoscale

Accepted Manuscript

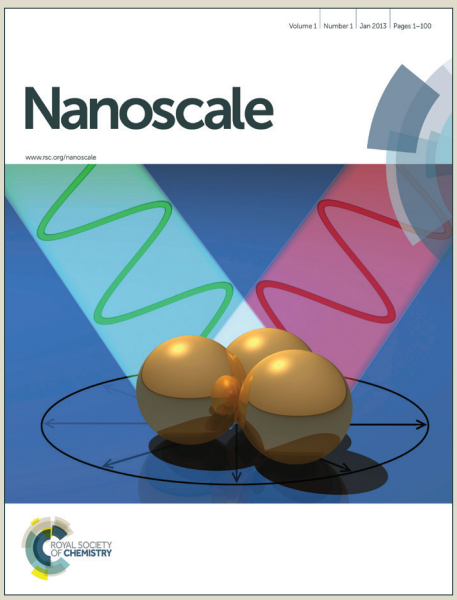

ROYAL SOCIETY OF CHEMISTRY

www.rsc.org/nanoscale

Nanoscale

RSCPublishing

Paper

Dynamic Observation on the Growth Behaviors in Manganese Silicide/Silicon Nanowire Heterostructures

Cite this: DOI: 10.1039/x0xx00000x

Received 00th January 2012,
Accepted 00th January 2012

DOI: 10.1039/x0xx00000x

www.rsc.org/

Yu-Hsun Hsieh, Chung-Hua Chiu, Chun-Wei Huang, Jui-Yuan Chen, Wan-Jhen Lin and Wen-Wei Wu*

Metal silicide nanowires (NWs) are of great interesting materials with diverse physical properties. Among these silicides, manganese silicides nanostructures have attracted wide attentions due to their several potential applications, including microelectronics, optoelectronics, spintronics and thermoelectric devices. In this work, we exhibited the formation of pure manganese silicide and manganese silicide/silicon nanowire heterostructures through solid state reaction with line contacts between manganese pads and silicon NWs. Dynamical process and phase characterization have been investigated by *in-situ* transmission electron microscopy (*in-situ* TEM) and spherical aberration corrected scanning transmission electron microscope (Cs-corrected STEM), respectively. The growth dynamics of manganese silicide phase under thermal effect were systematically studied. Additionally, Al_2O_3, served as the surface oxide, would alter the growth behavior of MnSi nanowire, involving enhancement of the silicide/Si epitaxial growth and effect of the diffusion process in silicon nanowire as well. In addition to fundamental science, the significant study would be great potential in advancing future processing techniques in nanotechnology and related applications.

Introduction

As the core of semiconductor technology, silicon-based devices are still the mainstream of the integrated circuits (IC) industry. Traditional manufacturing process utilized the top-down approach in which the devices or interconnects were fabricated by processes such as photolithography, thin-film deposition, etching, and metallization. However, according to Moore's law, the number of transistors on integrated circuits will double per 18 month. As the size of every devices may keep shrinking to below 10 nm, many fundamental devices will encounter the difficulties at small dimension.[1] Therefore, bottom-up process, such as self-assemble method, for the formation of 1D nanowire shed a light on leading to a new field of nanotechnology.

Transition-metal silicide nanowires have been subject of broad interest for their unique physical properties, good chemical stability, high quality interface with Si, excellent compatibility with Si device processing, and many superior functions available driven by the size effect.[2] Several synthetic approaches toward metal silicide NWs, including chemical vapor transport (CVT)[3, 4], chemical vapor deposition (CVD)[5-8], hydrothermal process[9] and solid state reaction[10-12], have been studied. Low resistivity metal silicide such as NiSi,[11, 13-15] $NiSi_2$[16] and PtSi[17, 18] NWs were fabricated for electric nano-device applications through solid state reaction, which is the chemical reaction caused by inter-diffusion of metal and Si atoms and subsequent phase transformation. This environmentally friendly way provides ability to control the heterostructures and silicide phases in nanowire without additional byproduct, which is of great significance.

Manganese silicides have seven different thermodynamically stable phases including Mn_6Si, Mn_4Si, Mn_3Si[19], Mn_5S_2, Mn_5Si_3[19], MnSi, and $MnSi_{2-x}$[20]. Among these phases, MnSi is an excellent magnetic contact material for magnetic applications[21-25] and spintronics such as spin-FET[26]. $MnSi_{2-x}$ has attracted wide attention for excellent thermoelectric properties owing to the low thermal conductivity of 2−4 W/m K and estimable Figure of merit (ZT) values up to 0.7−0.8.[27-29] In this work, solid state reaction was carried out to fabricate MnSi NWs which is an intermetallic compound with non-center symmetry B20-type cubic structure.[30] Also, MnSi is an itinerant ferromagnetic material. It was found to have a special helical magnetism when the temperature was lower than Curie temperature (T_c) at about 30K.[31, 32] A quantum critical phase transition will take place and bring magnetic skyrmion as a small magnetic field (~0.1-0.2T) is applied. Furthermore, MnSi performs a non-Fermi liquid behavior at high-pressure condition; thus, Mn silicide nanostructures are expected to have significant potential and wide interest in microelectronic, energy, optoelectronics, magnetic, spintronics and thermalelectric devices. To promote the efficiency of these devices, the ability to control the reactions is strongly desired. However, the related dynamic study of manganese silicide is still rare, which is of significant effort in this study. With the aid of *in-situ* TEM technique[10, 12, 14, 15, 33], reaction process can

be directly observed and controlled. Furthermore, the oxide shell structure plays a critical role to alter the crystal feature of Mn silicide. Some electric properties based-on Si/MnSi nano-heterostructures were also investigated, exhibiting promising potential in future advanced nanodevices.

Experimental

In this work, high aspect ratio of single crystalline silicon NWs were grown on a silicon wafer in the horizontal three zone furnace through vapor evaporation and deposition process with vapor–liquid–solid (VLS) mechanism (SEM and TEM images of silicon NWs can be referred to Supporting Information S1). After the growth process, Si wafer was immersed into an ethanol solution and as-grown Si NWs were detached by ultrasonic vibration. Then, Si NWs will be dispersed on the SiO_2/Si_3N_4 membrane samples and coated with the PMMA. Electron-beam lithography process was carried out to define the contact pads where manganese in 150 nm was deposited by E-gun evaporator at the following step. Prior to Mn evaporation, surface oxide will be removed by buffered hydrofluoric acid for 30 seconds. After lift-off process, the reaction devices were completely fabricated (Supporting Information S2).

The Si-Al_2O_3 core/shell nanostructure was prepared with an atomic layer chemical vapor deposition system. 20-nm-thick alumina was deposited at 250 ℃ with trimethylaluminum (TMA) as the source. The processing pressure in the chamber was 174~228 mtorr. In our processing, a total of 227 cycles was used, resulting in an alumina thickness of 20 ± 1 nm, which corresponds to an average growth rate of 0.88 Å per cycle. To prepare the specimens of the Si-Al_2O_3 core/shell nanostructure device covered with Mn pads, the as-grown Si nanowires were etched with HF prior to the Al_2O_3 coating, so that Al_2O_3-Si nanowires were obtained. Subsequently, the Mn pads were evaporated after the coated Al_2O_3 at defined regions were etched with HF. Solid state reaction through the contact pads and Si NWs was carried out by using Japan Electron Optics Laboratory 2000 V (JEOL-2000V) *in-situ* transmission electron microscope. The vacuum in the sample stage was about 3×10^{-10} torr. *In-situ* observation of the reaction process to form manganese silicide/silicon NW heterostructures was investigated at the temperature of 500 ± 10 ℃. The *in-situ* TEM was equipped with a video recorder which has a time resolution of 1/30 s. JEOL-ARM200F spherical aberration corrected scanning transmission electron microscope (Cs-corrected STEM) and Energy Dispersive Spectrometer (EDS) were used to identify the structure, morphology and composition of the Si NWs and manganese silicide NWs devices.

Results and discussion

The schematic illustration of the device configuration with Si NW covered by Mn pads and the formation of Mn silicide/Si/Mn silicide nano-heterostructures are shown in Fig. 1(a). Fig. 1(b) and Fig. 1(c) are TEM images of NW before and after solid-state reaction with line contact between Mn electrode pads and Si NW at 500 ℃, respectively. Within the nanowire, darker regions are MnSi while the brighter regions are remained Si NW, and two clear interfaces, between silicon and Mn silicide, are indicated by two arrows in Fig. 1(c). According to the high-resolution lattice image in Fig. 1(d), we identify this phase as mono-manganese silicide. The inset shows the corresponding fast Fourier transformed diffraction pattern with [121] zone axis. EDS mappings were performed to verify that Mn actually diffuse into Si NWs (Supporting Information S3).

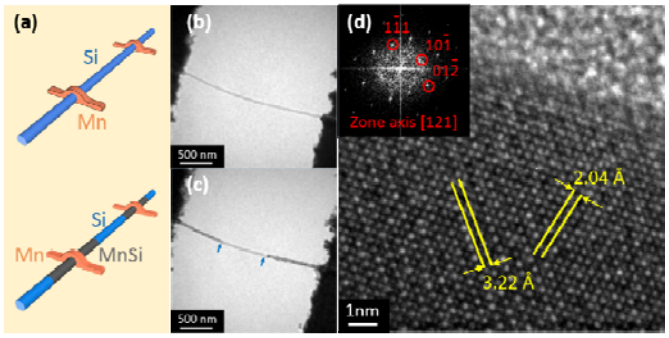

Fig. 1 (a) Schematic illustration of the device configuration with Si NW covered by Mn pads and the formation of Mn silicide/Si/Mn silicide nano-heterostructures. (b) TEM image of Si NW and Mn pads. (c) TEM image of the device after annealing at 500 ℃. The arrows indicate the reaction interface of Si and Mn silicide. (d) HRTEM image of MnSi and inset shows the corresponding FFT diffraction pattern with [121] zone axis.

Fig. 2(a)-2(f) are a series of images recorded from the video showing the formation process of the solid state reaction between manganese and silicon NW at 500 ℃. These images were obtained at elapsed times of (a) 0:00, (b) 1:22, (c) 2:05, (d) 3:07, (e) 4:24, and (f) 5:26, indicated at the lower right corners. The first number is in units of minutes and the following two numbers are in units of seconds. As time goes by, manganese atoms diffuse into Si NW, solid-state reaction occurs to form MnSi and it keeps growing along the axial-direction of the Si nanowire.

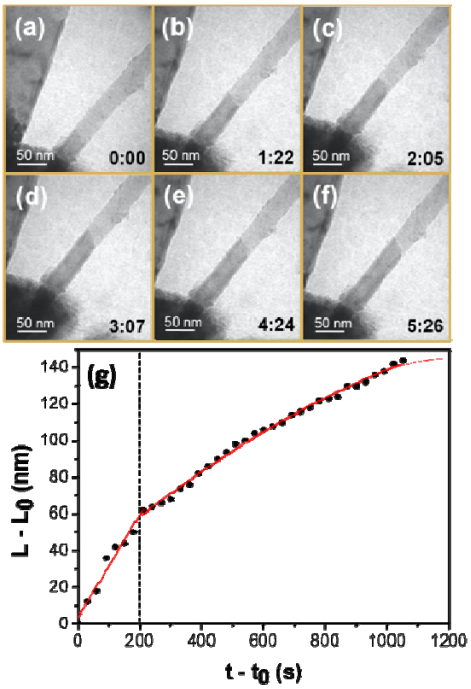

Fig 2 A series of images from the video showing the formation process of the solid-state reaction of Mn and Si. The images were obtained at elapsed times of (a) 0:00, (b) 1:22, (c) 2:05, (d) 3:07, (e) 4:24, and (f) 5:26. The first number is in units of minutes and the following two numbers are in units of seconds. (g) The plot of MnSi reaction length as a function of time. The linear to non-linear transition is indicated by black dashed line.

Fig. 2(g) is the plot of MnSi reaction length as function of time. L_0 is the critical length at which the clear MnSi/Si interface was firstly observed. Red line is the fitting curve, illustrating two different growth rates in the solid-state reaction of Mn and Si NWs. The growth rate was faster and roughly linearly at the beginning of the reaction but slowed down and trended into parabolic growth at the following step. It means that the growth process was mainly controlled by interface-limited reaction instead of diffusion-limited reaction at the first stage. However, since the diffusivity coefficient of Mn in Si and MnSi are different, the diffusion rate of manganese atoms into silicon is much faster than that into silicide. Therefore, the linear growth rate may slow down and transform into parabolic behavior after reaction about 200 seconds. Additionally, from this curve, the average reaction rate along the axial direction was calculated to be 0.30 nm/s for the first stage.

TEM image around MnSi/Si interface is shown in figure 3(a). After the annealing process at 500 ℃, MnSi with polycrystalline nature was obtained, the growth front of the silicide would develop the curved interface with newly nucleation site near the surface. This phenomenon could be better understood through the *in-situ* video (Supporting Information Video-1).

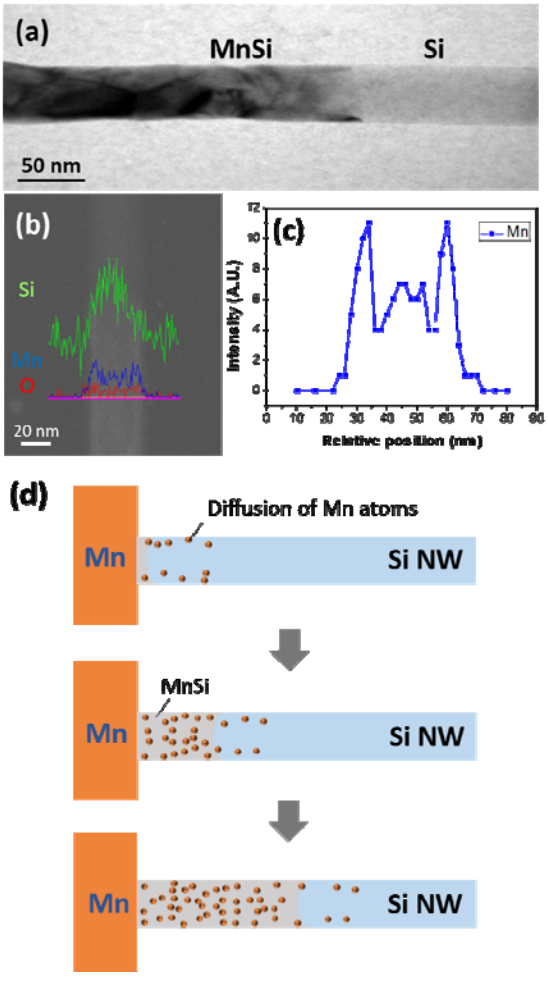

Fig. 3 (a) TEM image around the MnSi/Si interface. (b) EDS line scan at the front end of MnSi. (c) High-magnification of EDS line scan profile for the Mn element in figure (b). (d) A schematic drawing of MnSi formation process.

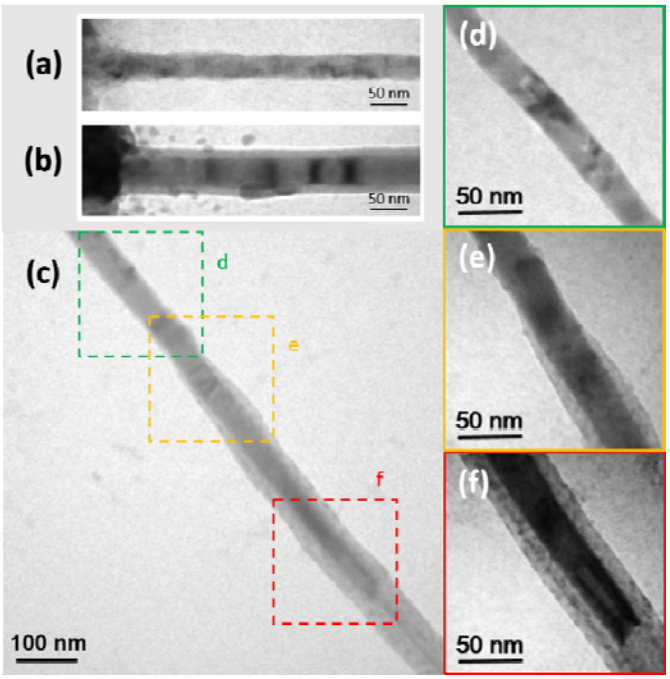

Fig. 4 The influence of surface oxide on the growth of MnSi nanowire. (a) and (b) Two Si nanowires in similar diameters without/with oxide coated on the surface. (c) MnSi grown in bare silicon first and then into the oxide-confined. (d-f) high-magnification image of the highlights area in (c).

When the solid state reaction occurred, two edges of nanowire took the lead in changing the contrast, indicating that the first reaction position may take place at the surface of NW. After a few seconds, the center of NW begins to react. As a consequence, we suggest that Mn and Si might first react and nucleate at the surface of NWs. The possible reason for this diffusion behavior is that there are more defects at the surface. These defects such as dislocations provide the heterogeneous nucleation site with a higher free energy. The diffusion behavior schematic illustration was shown in Fig. 3(d). To further investigate this phenomenon, EDS line scan was carried out at the front end of the as-formed MnSi as shown in Fig. 3(b). Fig. 3(c) is the high-magnification of EDS line scan profile for Mn element in Fig. 3(b). It shows that the intensity at the two edges is obviously higher than that at center region, consistent with our conjecture of the diffusion behavior.

Since the MnSi nanowires formed were polycrystalline, we tried to introduce the effect of surface oxide on the growth of MnSi nanowire. Expected that MnSi could form as single crystalline, so we designed an experiment where two nanowires with similar diameters but only one nanowire was coated by oxide and the other as the control group as shown in Fig. 4(a) and Fig. 4(b), respectively. After 500 ℃ annealing, polycrystalline MnSi was formed in the bare silicon NW, whereas single-crystalline MnSi was observed in the alumina oxide/shell nanowires. To further examine the effect of oxide shells, another experiment was carried out. MnSi first reacts into bare silicon and then into the oxide/shelled region where compressive stress was applied by the shell indicated in Fig. 4(c). Figs. 4(d)-4(f) are high-magnification images of the highlights area in Fig. 4(c). It is found that MnSi is polycrystalline structure in the bare silicon region. However, once MnSi reacts into the oxide/shelled region, it starts to form single crystalline MnSi as shown in Fig. 4(e) and Fig. 4(f).

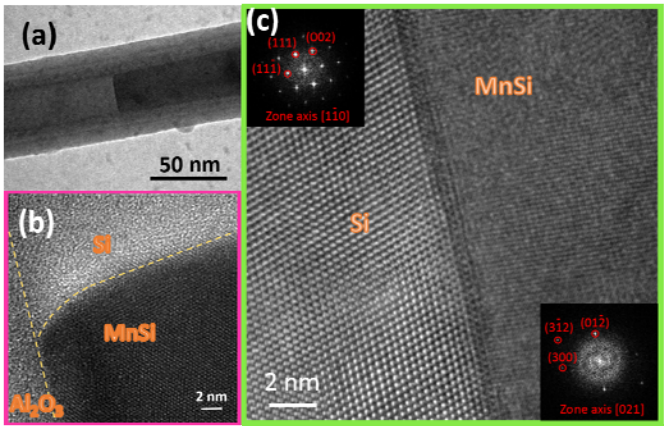

Fig. 5 (a) TEM image of the Si/MnSi interface when oxide-shell was applied. (b) HRTEM image of MnSi after annealed at 500 ℃ shows a curved interface near the oxide edge. (c) HRTEM image of Si/MnSi heterojunction. The insets show the FFT diffraction patterns of Si and MnSi, respectively.

The single crystalline transition may attribute to two reasons. One is the surface energy of Al_2O_3/MnSi generates a higher net free energy and impedes surface nucleation. The other is the oxide/shells structure with compressing effect, which would restrain the nucleation rate and the number of nuclei in the cross-sectional area of the NWs.

In addition to single crystal growth, Fig. 5(a) shows a TEM image with a sharp and clear silicon/silicide interface when single crystal MnSi grows into Si/Al_2O_3 core/shell nanowire. The growth kinetics of Mn silicide in Si/Al_2O_3 NW template was investigated through dynamic observation by *in-situ* TEM (Supporting Information Video-2 and Video-3). In our observation, the radial growth of MnSi starts from the center rather than from the edge of the nanowire. Furthermore, an image of triple point and high-lighted with dash lines at the boundary of Si, Al_2O_3 and MnSi after being annealed at 500 ℃ are clearly found as shown in Fig. 5(b). This is supposed that the surface energy of the oxide–silicide interface is higher than that of the oxide–silicon interface, indicating Al_2O_3 plays major role in the growth dynamics[34]. Therefore, when every new Mn silicide atomic layer approaches the edge of the Si NW, high-energy barrier will impede the reaction before the edge transformed to the oxide/silicide interface, leading to a curvature presented near the edge of Si/oxide interface during the growth process. This result also suggests that the nucleation mechanism was center-nucleation (homogeneous) rather than edge-nucleation (heterogeneous) owing to the variation in the net change of free energy demonstrated in our previous studies[12, 34, 35]. Moreover, we find some lattice relations across the interface between Si and MnSi, which is also attributed to the compressive stress from the oxide/shell structure. The HRTEM image shows the epitaxial relations between Si and MnSi are $[1\bar{1}0]$//[021] and $(11\bar{1})$//(300). The insets are their corresponding FFTs with $[1\bar{1}0]$ and [021] zone axis, respectively. Therefore, the Si/Al_2O_3 core/shell structure not only play an important role in confining the growth of single crystal MnSi but also change the diffusion behavior of Mn in formation of MnSi, and promote the formation of MnSi to maintain the epitaxial relationships between Si and MnSi as well. Moreover, the growth rate of the MnSi in the Al_2O_3-coated Si nanowire along the axial direction is linear with about 1.94 nm/s (Figure S4), significantly different from that in bare Si nanowire. It may be attributed to several factors in combination of oxide compressive effect, contact quality between Mn and Si nanowires, and diameter of Si channel as well.

At the area near the Mn pad-MnSi interface, no matter whether the Si nanowires were coated with oxide or not, no other phases were observed. The nanowires only consist of pure MnSi phase even when the Si nanowire were completely transformed. Figure S5 shows the TEM images and high-resolution TEM images of both systems (bare Si and Al_2O_3-coated Si nanowires).

In addition to the study of growth behaviors, some electric properties have been investigated. MnSi NW with the resistivity of 533 μΩ-cm by two-terminal measurement was calculated and showed in supporting information S6. The true value may be lower if the contact resistance was excluded. The electron transport measurement devices based-on Si/MnSi nano-heterostructures with different silicon channel lengths were also fabricated (Supporting Information S7). From the I-V measurement, MnSi/Si nanowire heterostructures exhibit the Schottky-diode-like (SDL) behavior. The result shows that the current increases as the channel length decreases and we calculate the effective barrier height ψ_B with a value of 0.42 eV. The schematic illustration of band diagram is also shown in supporting information S6.

Conclusions

In this work, we have successfully fabricated both of MnSi nanowires and MnSi/Si/MnSi nanowire heterostructures at 500 ℃ through solid-state reaction. The *in-situ* observations provided information on the growth progress and kinetic mechanism. The plot of the growth rate suggests that MnSi has a linear to non-linear transition behavior in bare Si system due to the different diffusivity of the Mn atom in Si and silicide. When Mn diffuse into bare Si NW and subsequently react with silicon, the first MnSi will form at the surface of NW and perform as a polycrystalline structure. As Al_2O_3 oxide-shell is applied, compressive stress will driven MnSi to be single crystalline with a sharp Si/MnSi interface. The Si/Al_2O_3 core-shell structures not only enhance the silicide/Si epitaxial growth but also modify the diffusion process from edge-nucleation (heterogeneous) to center-nucleation (homogeneous) in silicon nanowire. Furthermore, we have also made some electrical properties measurements based on MnSi NW and MnSi/Si/MnSi nanowire heterostructure. Our significant study would provide the understanding and potential applications for future processing techniques in nanotechnology.

Acknowledgements

W.W.W. acknowledge the support by Ministry of Science and Technology through grants 103-2221-E-009 -056 -MY2 and 103-2221-E-009 -222 -MY3

Notes and references

[a] *Department of Materials Science and Engineering, National Chiao Tung University, No.1001, University Rd., East Dist., Hsinchu City 300, Taiwan. E-mail: wwwu@mail.nctu.edu.tw; Fax: +886-3-5724727; Tel: +886-3-5712121-55395*

† Electronic Supplementary Information (ESI) available: [Five ESI to demonstrate the SEM and HRTEM images of silicon nanowires, the fabrication procedures of *in-situ* TEM samples, EDS mapping of Mn silicide/Si/Mn silicide nanowire heterostructures, I-V measurement of MnSi NW and electrical properties measurement of Mn silicide/Si/Mn silicide nanowire heterostructures samples. Three *in-situ* videos as ESI to present dynamic observation of the formation of MnSi nanowires]. See DOI: 10.1039/b000000x/

1. B. Yu and M. Meyyappan, *Solid-State Electronics*, 2006, 50, 536-544.
2. H. Jiang, C. M. Osburn, P. Smith, Z. G. Xiao, D. Griffis, G. McGuire and G. A. Rozgonyi, *Journal of The Electrochemical Society*, 1992, 139, 196-206.
3. Y. Song, A. L. Schmitt and S. Jin, Nano Letters, 2007, 7, 965-969.
4. J. R. Szczech, A. L. Schmitt, M. J. Bierman and S. Jin, *Chemistry of Materials*, 2007, 19, 3238-3243.
5. Y. H. Liang, S. Y. Yu, C. L. Hsin, C. W. Huang and W. W. Wu, *Journal of Applied Physics*, 2011, 110, 074302.
6. C. Y. Lee, M. P. Lu, K. F. Liao, W. F. Lee, C. T. Huang, S. Y. Chen and L. J. Chen, *The Journal of Physical Chemistry C*, 2009, 113, 2286-2289.
7. B. Xiang, Q. X. Wang, Z. Wang, X. Z. Zhang, L. Q. Liu, J. Xu and D. P. Yu, *Applied Physics Letters*, 2005, 86, 243103.
8. H. K. Lin, Y. F. Tzeng, C. H. Wang, N. H. Tai, I. N. Lin, C. Y. Lee and H. T. Chiu, *Chemistry of Materials*, 2008, 20, 2429-2431.
9. J. Ma, Y. Gu, L. Shi, L. Chen, Z. Yang and Y. Qian, *Journal of Alloys and Compounds*, 2004, 376, 176-179.
10. K. C. Lu, W. W. Wu, H. W. Wu, C. M. Tanner, J. P. Chang, L. J. Chen and K. N. Tu, *Nano Letters*, 2007, 7, 2389-2394.
11. K. C. Lu, K. N. Tu, W. W. Wu, L. J. Chen, B. Y. Yoo and N. V. Myung, *Applied Physics Letters*, 2007, 90, 253111.
12. C. H. Chiu, C. W. Huang, J. Y. Chen, Y. T. Huang, J. C. Hu, L. T. Chen, C. L. Hsin and W. W. Wu, *Nanoscale*, 2013, 5, 5086-5092.
13. Y. Wu, J. Xiang, C. Yang, W. Lu and C. M. Lieber, *Nature*, 2004, 430, 61-65.
14. W. W. Wu, K. C. Lu, C. W. Wang, H. Y. Hsieh, S. Y. Chen, Y. C. Chou, S. Y. Yu, L. J. Chen and K. N. Tu, *Nano Letters*, 2010, 10, 3984-3989.
15. W. W. Wu, K. C. Lu, K. N. Chen, P. H. Yeh, C. W. Wang, Y. C. Lin and Y. Huang, *Applied Physics Letters*, 2010, 97, 203110.
16. Y. C. Lin, Y. Chen, D. Xu and Y. Huang, *Nano Letters*, 2010, 10, 4721-4726.
17. K. C. Lu, W. W. Wu, H. Ouyang, Y. C. Lin, Y. Huang, C. W. Wang, Z. W. Wu, C. W. Huang, L. J. Chen and K. N. Tu, *Nano Letters*, 2011, 11, 2753-2758.
18. Y. C. Lin, K. C. Lu, W. W. Wu, J. Bai, L. J. Chen, K. N. Tu and Y. Huang, *Nano Letters*, 2008, 8, 913-918.
19. J. M. Higgins, R. Ding and S. Jin, *Chemistry of Materials*, 2011, 23, 3848-3853.
20. J. M. Higgins, A.L. Schmitt, I. A. Guzei and S. Jin, *Journal of the American Chemical Society*, 2008, 130, 16086-16094.
21. N. Manyala, Y. Sidis, J. F. DiTusa, G. Aeppli, D. P. Young and Z. Fisk, *Nature*, 2000, 404, 581-584.
22. C. Pfleiderer, S. R. Julian and G. G. Lonzarich, *Nature*, 2001, 414, 427-430.
23. F. Jonietz, S. Mühlbauer, C. Pfleiderer, A. Neubauer, W. Münzer, A. Bauer, T. Adams, R. Georgii, P. Böni, R. A. Duine, K. Everschor, M. Garst and A. Rosch, *Science*, 2010, 330, 1648-1651.
24. H. Du, J. P. DeGrave, F. Xue, D. Liang, W. Ning, J. Yang, M. Tian, Y. Zhang and S. Jin, *Nano Letters*, 2014, 14, 2026-2032.
25. X. Yu, J. P. DeGrave, Y. Hara, T. Hara, S. Jin and Y. Tokura, *Nano Letters*, 2013, 13, 3755-3759.
26. Y. C. Lin, Y. Chen, A. Shailos and Y. Huang, *Nano Letters*, 2010, 10, 2281-2287.
27. M. I. F. Ikuto Aoyama, Vladimir K. Zaitsev, Fedor Yu. Solomkin, Ivan S. Eremin, Aleksandr Yu. Samunin, Mika Mukoujima, Seijiro Sano and Toshihide Tsuji, *Japanese Journal of Applied Physics*, 2005, 44, 8562-8570.
28. I. K. Aoyama, H.; Rauscher, L.; Kanda, T.; Mukoujima, M.; Scano, S.; Tusji, T., *Jpn. J. Appl. Phys*, 2005, 44, 4275-4281.
29. A. Pokhrel, Z. P. Degregorio, J. M. Higgins, S. N. Girard and S. Jin, *Chemistry of Materials*, 2013, 25, 632-638.
30. H. Liu, G. She, X. Huang, X. Qi, L. Mu, X. Meng and W. Shi, *The Journal of Physical Chemistry C*, 2013, 117, 2377-2381.
31. J. M. Higgins, R. Ding, J. P. DeGrave and S. Jin, *Nano Letters*, 2010, 10, 1605-1610.
32. K. Seo, H. Yoon, S.-W. Ryu, S. Lee, Y. Jo, M.-H. Jung, J. Kim, Y. K. Choi and B. Kim, *ACS Nano*, 2010, 4, 2569-2576.
33. Y. C. Chou, W. W. Wu, S.-L. Cheng, B. Y. Yoo, N. Myung, L. J. Chen and K. N. Tu, *Nano Letters*, 2008, 8, 2194-2199.
34. Y. C. Chou, W. W. Wu, L. J. Chen and K. N. Tu, *Nano Letters*, 2009, 9, 2337-2342.
35. Y. C. Chou, W. W. Wu, C. Y. Lee, C. Y. Liu, L. J. Chen and K. N. Tu, *The Journal of Physical Chemistry C*, 2010, 115, 397-401.